Chapter 9

Chemically Exfoliated Graphene Nanosheets for Flexible Electrode Applications

Joong Tark Han, Seung Yol Jeong,
Hee Jin Jeong and Geon-Woong Lee

Additional information is available at the end of the chapter

http://dx.doi.org/10.5772/intechopen.77284

Abstract

Graphene oxide (GO), produced by oxidation of graphite powder and exfoliation, is intensively utilized in electrodes, templates for hybrid materials, interfacial modifiers, three-dimensional structures, and so on, with its performance as an electrode material being determined by its chemical and structural states. This chapter describes the fabrication method of GO nanosheets from graphite oxide powder and their stable dispersion after reduction and applications in devices. Rheologically driven exfoliation and unusual acoustic cavitation methods were applied to produce large and less defective GO nanosheets. As a dispersion strategy of reduced GO (RGO) in solution, TiO_2 precursor, cation-π interaction, silanol groups were introduced. Moreover, supramolecular chemistry, for example, quadruple hydrogen bonding moieties, was applied to solve the dispersion of highly concentrated RGO pastes. As potential applications of GO and RGO, we described GO as a p-type dopant and interfacial modifier as well as energy storage electrodes, IR sensors, and emitters. The judicious use of chemically exfoliated graphene can open new applications as a flexible electrode.

Keywords: graphene oxide, reduced graphene oxide, exfoliation, dispersion

1. Introduction

Atomically thin graphene oxide (GO), produced by oxidation and exfoliation of graphite powder, has been intensively studied for applications in electrodes, templates for hybrid materials, interfacial modifiers, three-dimensional structures, and so on [1–4]. Its performance as an electrode material is determined by its chemical and structural states. The topological defects present in the basal plane of reduced GO (RGO) can significantly affect its electrical and electrochemical

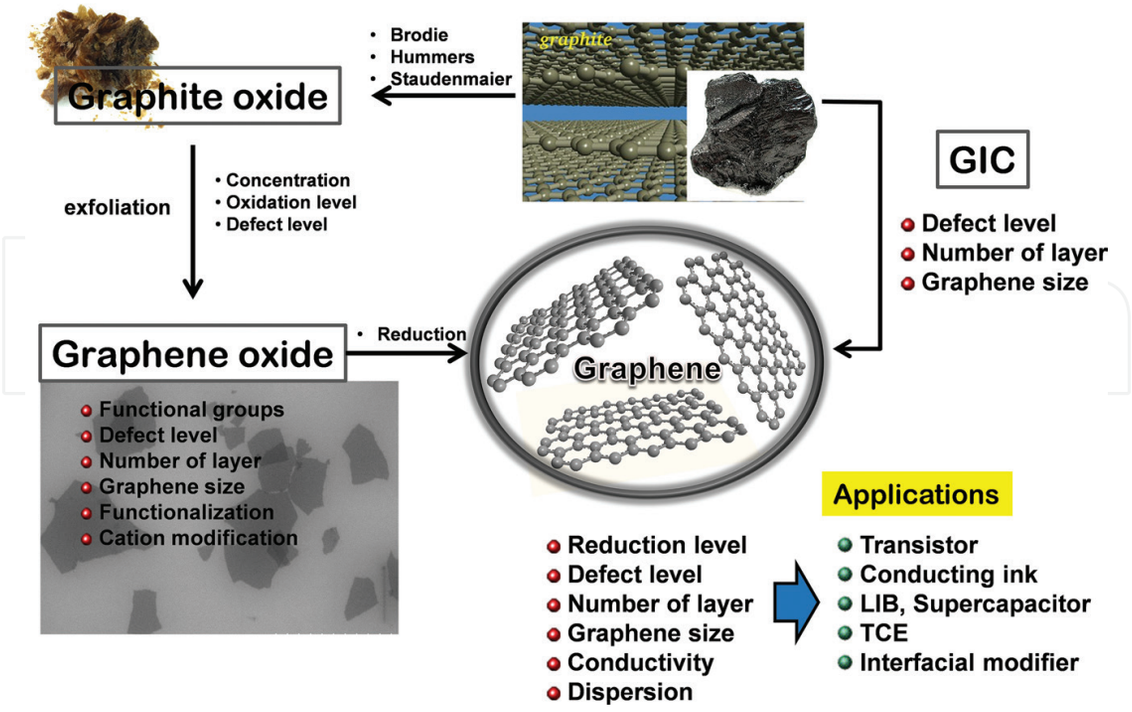

Figure 1. Production schematics of chemically exfoliated graphene from graphite. Here, GIC stands for graphite intercalation compound and LIB for lithium ion batteries.

properties. As shown in **Figure 1**, GO nanosheets are typically produced by oxidizing graphite using strong acids and oxidants, followed by exfoliation in aqueous solutions [5–8]. It should be noted that, the characteristics of GO and RGO nanosheets critically depend on the oxidation states of graphite oxide and its exfoliation. Moreover, for real-life applications, the dispersion stability of RGO inks or pastes is a prerequisite. The dispersion of high-quality chemically exfoliated graphene (CEG) or RGO in polar solvents, which contain few oxygen functional groups and defects, has been impossible due to the hydrophobic nature of graphene without post treatment or addition of dispersant molecules. The stability of RGO dispersion is one of the crucial factors for preserving their unique properties such as electrical conductivity and mechanical strength.

Therefore, this chapter describes some of the research on CEG nanosheets conducted over the past 8 years that addresses these and other challenges, with an emphasis on our own efforts. We began with the efficient fabrication method of single layer GO nanosheets from graphite, and then described the stable dispersion of RGO in solutions. Furthermore, we described the applications of GOs as p-type dopants, conductors and interfacial modifiers. We concluded with some discussion of future directions and the remaining challenges in chemically exfoliated graphene technologies.

2. Efficient fabrication of single layer graphene oxide nanosheets

2.1. Rheologically driven exfoliation of graphite oxide

Conventional sonicators vigorously destroy the structure of GO, which results in producing small-sized GO nanosheets due to acoustical wave agitation in solution. An alternative way

to minimize the destructive effect of exfoliation of graphite oxide is to use a homogenizer to apply a shear force in the solution (**Figure 2(A)**). The average lateral size of sonicated GO (SGO) nanosheets (a few square micrometers) was smaller than that of the homogenized GO (HGO) nanosheets (a few hundred square micrometers) in the optical images in **Figure 2(B)** and **(C)**. The SGO nanosheets exhibited some agglomerated GO on the silicon substrate due to the small size distribution of the sheets. To confirm the exfoliation effects of HGO and SGO sheets, we carried out homogeneous dispersion of GO sheets in aqueous solution without using small size graphite powder (70 μm). The rheologically derived or sonicated exfoliation and dispersion of GO sheets was accomplished (**Figure 1(d)**) in an aqueous NaOH solution at pH 10 for 1 h. After diluting it using dimethylformamide (DMF), the RGO solution was prepared by chemical reduction with hydrazine for preparing transparent conducting films. The enhanced sheet resistance of the reduced HGO (HRGO) thin film was found to be 2.2 kΩ/sq. at 80% transmittance. The effective exfoliation method has great potential for application for high performance GO-based flexible electrodes.

2.2. Extremely efficient liquid exfoliation of graphite oxide using unusual acoustic cavitation

Acoustic cavitation, also called sonication, has been used to fabricate two-dimensional (2-D) nanosheets via exfoliation of bulk-layered crystal materials in solution to fabricate fascinating materials such as graphene, transition metal dichalcogenides, and transition metal oxides. The

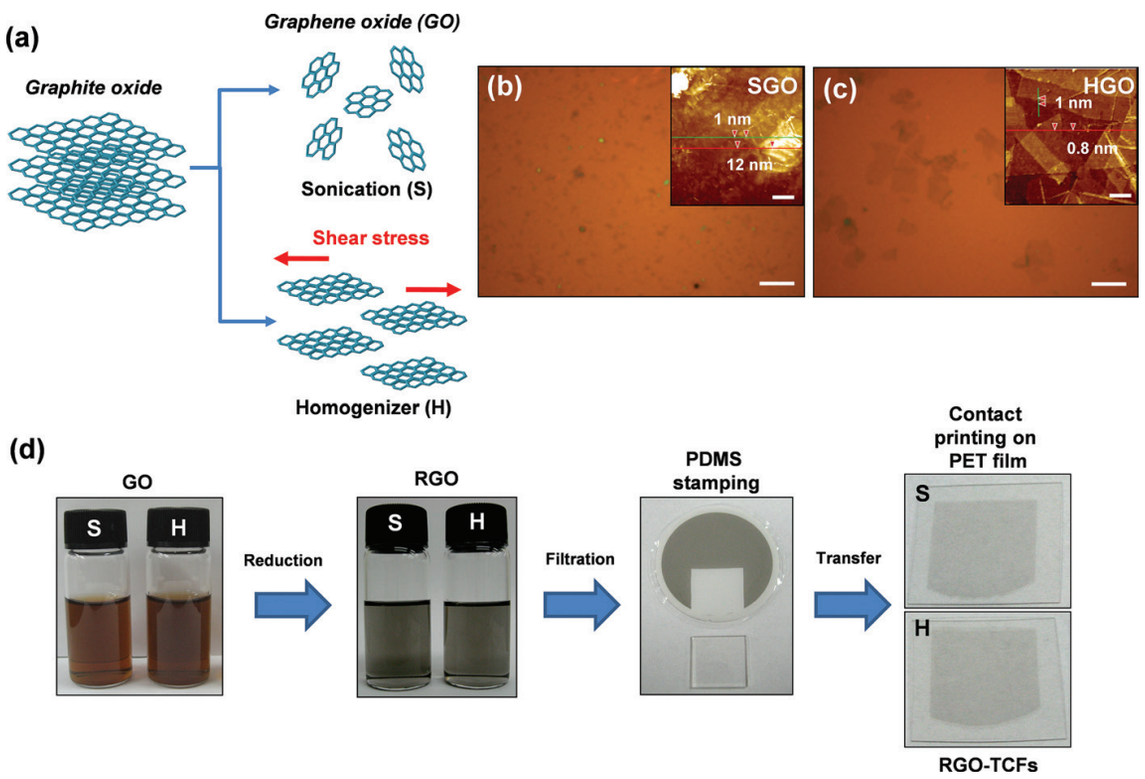

Figure 2. Fabrication of GO and RGO nanosheets by using different exfoliation methods. (A) Exfoliation of graphite oxide by sonication (S) or homogenization (H). (B) and (C) optical images of GO samples prepared by sonication (B) and homogenization (C) deposited on a 300-nm-thick SiO2 substrate (inset: AFM images of the GO sheets). (D) Fabrication of transparent conducting films (TCFs) with RGO nanosheets by the contact printing of filtrated RGO films. Here PDMS is polydimethylsiloxane, PET is polyethylene terephthalate, and RGO-TCFs are reduced graphene oxide transparent conductive films. The scale bars in (B) and (C) are 10 μm, and those in the respective insets are 2 μm [9].

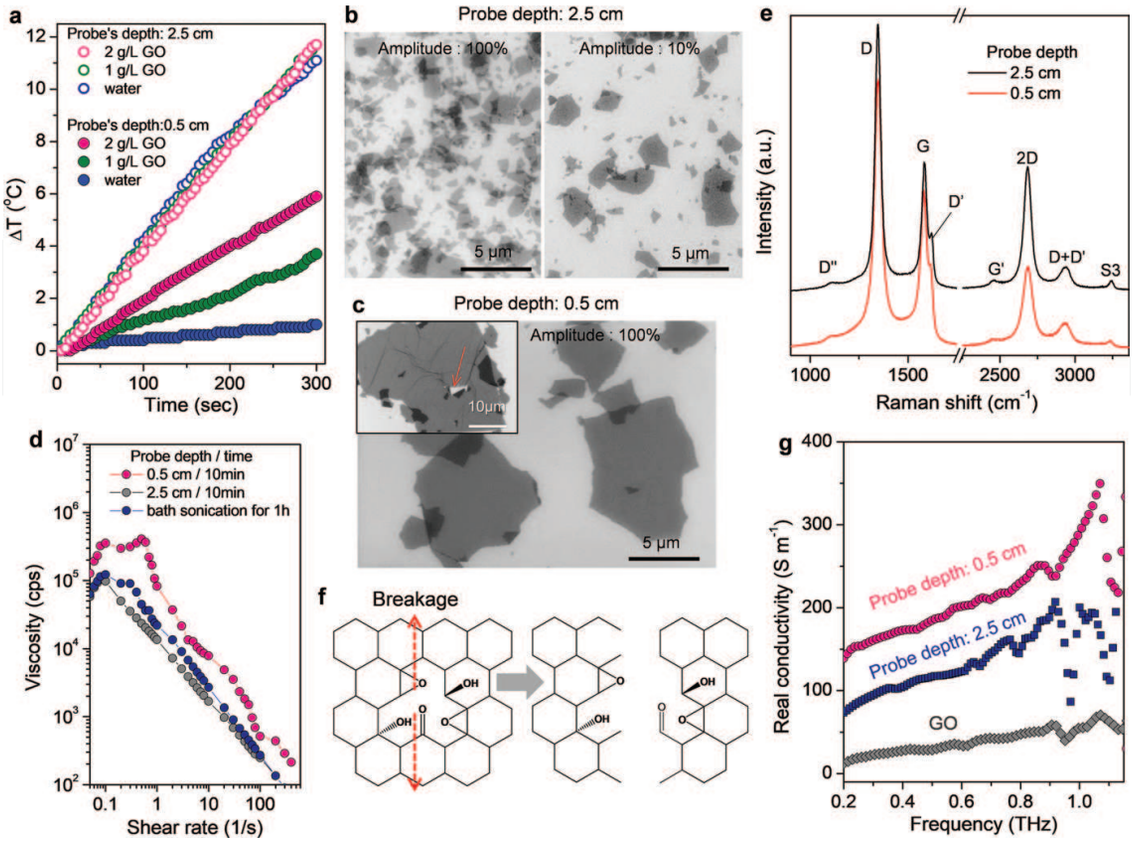

Figure 3. (a) Temperature change (ΔT) over time during sonication of pure water and of a GO suspension containing different initial amounts of graphite oxide. (b) and (c) FESEM images of GO nanosheets fabricated using probe sonication by dipping probe into the liquid surface by 2.5 and 0.5 cm, respectively, for 10 min. The large GO nanosheet was fabricated at 0.5 probe depth condition. (d) Shear viscosity of GO paste samples showing different rheological behavior due to their sizes. (e) Raman spectra of the chemically reduced GO nanosheets demonstrating the effect of acoustic cavitation at different probe depth on the crystalline structure of RGO (f) breakage of GO nanosheet initiated at the defect site or from the sp^3 hybridized region during probe sonication. (g) Real THz conductivity of the GO, SRGO, and LRGO films prepared by sonication with probe depths of 0.5 and 2.5 cm [13].

high energetic transient acoustic cavitation; the formation, growth, and implosive collapse of bubbles at high ultrasonic intensities (10–30 W cm^{-2}) in a liquid medium, allow to give physical effects on exfoliation of layered materials. However, the high energetic transient cavitation phenomenon can give a detrimental effect on 2D materials by generating defects on the surface, which decrease their electrical and other useful properties. Recently large (>10 μm) chemically modified graphene nanosheets have been developed from graphite oxide. These have fewer defects than those produced by other methods without requiring further separation processes and can be produced by combining ultrasonic acoustic cavitation with sufficient acoustic shearing and additional microbubbling by aeration in an extremely short time (10 min). It can be achieved by adjusting the ultrasound parameters (amplitude, time, and probe immersion depth) for the delivered power (related to temperature change (ΔT) **Figure 3(a)**), the acoustic flow rate, and the bubbling behavior in 200 mL water using conventional flat tip probes with a 12.7 mm diameter. In order to reduce the detrimental effect of transient cavitation, the probe tip was located at a 0.5 cm depth. Subsequently, the acoustic flow rate decreased from 0.62 to 0.47 m s^{-1} and then increased to 0.73 m s^{-1} at 100% amplitude, which was faster than the 10%

amplitude at the 2.5 cm probe depth. Moreover, bubbling due to the liquid surface instability under acoustic oscillation is also helpful for the efficient exfoliation of graphite oxide. Bubbling by aeration at the liquid surface is also helpful for the dispersion of nanomaterials because bubbling can produce a greater shearing effect on the particles in suspension under an acoustic flow with lower energy. **Figure 3(b)** and **(c)** shows the scanning electron microscopy (SEM) images of exfoliated GO nanosheets under different cavitation conditions. The maximum size of GO was dramatically increased by adjusting the probe depth from 2.5 to 0.5 cm. At a probe depth of 2.5 cm, the lateral size of GO was less than 5 μm even at 10% amplitude after 10 min of sonication (**Figure 3(b)**) because of breakage in the stretched C–C or C–O–C bonds [10, 11] due to the high energetic physical phenomena of microjets and shock waves [12]. However, at a probe depth of 0.5 cm, GO nanosheets with a maximum 30 μm size were produced even at the high output power setting (amplitude 100%) by reducing the detrimental effect of the high energy cavitation process (**Figure 3(c)**).

3. Dispersion of reduced graphene oxide

3.1. TiO_2 precursor-assisted dispersion of reduced graphene oxide in solution

The problems associated with the aggregation of the RGO sheets in organic solvents were addressed by introducing noncovalent interactions among the sp^2 carbons of the RGO sheets and the TiO_2 precursor sol, as shown in **Figure 4(a)**. Titanium dioxide is also a promising charge screening candidate because it can interact electrostatically with oxygen moieties causing charge trapping [14, 15]. The TiO_2 precursor sol was prepared from a titanium isopropoxide (TIP)/acac stabilizer (1/5 molar ratio) solution, which was added to the GO solution. In order to determine the minimum amount of used TiO_2 precursor for RGO dispersion, the varying amount of TiO_2 precursor sols were added into the GO solution prior to hydrazine reduction. The weight ratio between GO and TIP in the precursor TiO_2 sol was varied between 0 and 1.5. Just a 0.1 weight ratio was required to stabilize the RGO solution in dimethylformamide (DMF) after hydrazine reduction. This stable RGO/TiO_2 precursor sol mixture can be deposited onto the large area substrate by air-spraying without postreduction process. Usually, RGO films are fabricated by deposition of GO nanosheets on the substratem, followed by thermal or chemical reduction at elevated temperatures. Moreover, direct deposition of RGO solution onto the substrate induces formation of wrinkled structures, which can decrease their electrical properties. However, wrinkle-free RGO/TiO_2 hybrid multilayer films can be built up on SiO_2 by automatic spray-coating. The electrical transport characteristics of the RGO and RGO/TiO_2 hybrid films were investigated by preparing graphene field-effect transistors (FETs) on heavily doped Si substrates, which are commonly employed as gate electrodes. It is worth noting that the conductivity of the RGO film at the neutral charge point was maximized for GO/TIP (1/0.7 ratio) by inserting a thin TiO_2 layer into the RGO multilayer film, despite the amorphous insulating characteristics of TiO_2. This was due to the hole-doping effect caused by increasing the TiO_2 amount between the RGO nanosheets, which was demonstrated by observing a significant blue shift of the G peaks in Raman spectra.

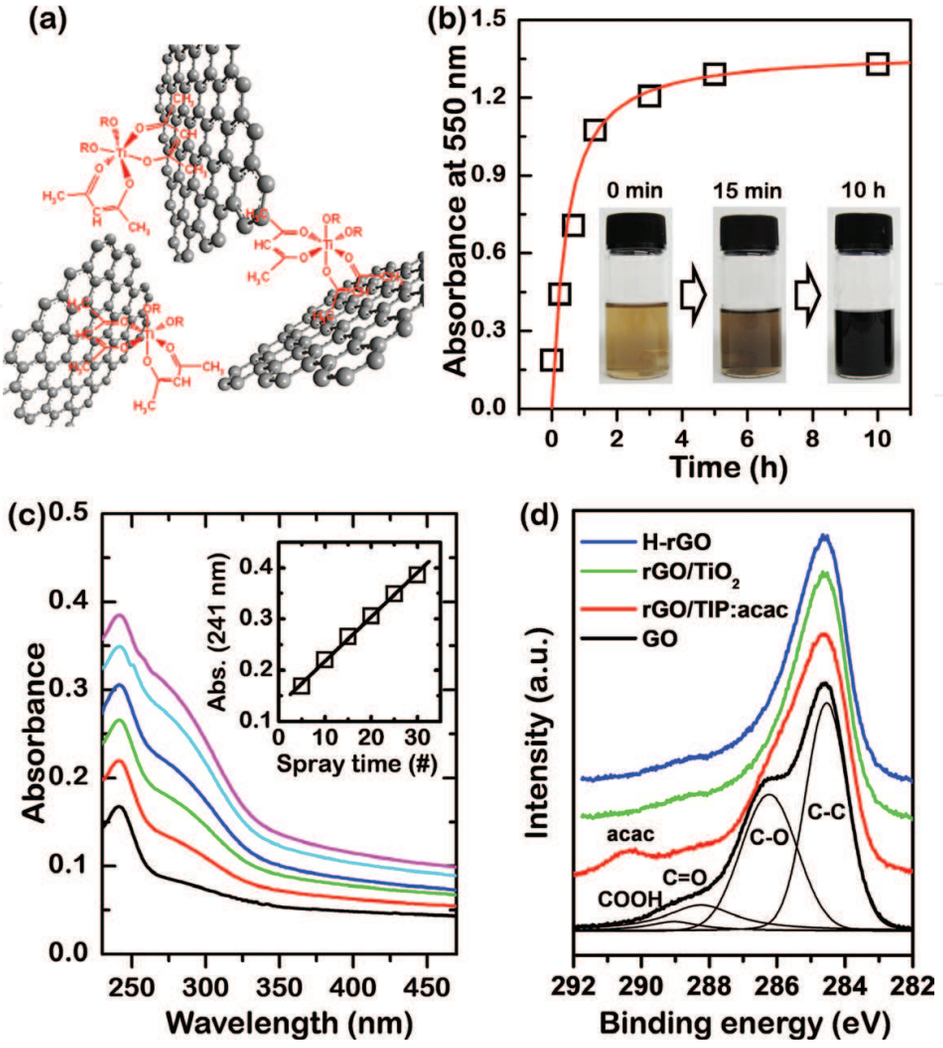

Figure 4. (a) Proposed mechanism for the dispersion of RGO sheets by the TiO_2 precursor sol via a hydrophobic interaction. (b) Dispersion stability of RGO solution in DMF after chemical reduction with hydrazine monohydrate; gradual increase of absorbance of GO solution at 550 nm and vial images shows the stable dispersion of RGO dispersion. (c) UV–Vis absorption spectra of RGO/TiO_2 hybrid multilayer films; the linear increase of absorption intensity shows the regular deposition of films by spraying. (d) C1s XPS spectra of GO, RGO reduced by hydrazine vapor (H-RGO), RGO/TIP:acac (TiO_2 precursor), and RGO/TiO_2 hybrid film thermally treated at 200°C [16].

3.2. Dispersion of reduced graphene oxide nanosheets by monovalent cation-π interaction

The cation-π interaction on crystallized RGO, which has fewer defects and oxygen functional groups, can be enhanced the dispersion stability in various solvents due to Coulombic repulsion between the cations on the in-plane of graphene. (Jeong et al. [17]) **Figure 5** shows the stable dispersion of RGO by monovalent cation–π interactions. The interactions did not directly occur on the basal plane of GO because the cations usually interact with the oxygen functional groups of highly oxidized GO (as described in **Figure 5(a)–(c)**). In order to effectively activate the cation interaction on π stage, the sp^2 carbon state on the basal plane is exposed through the reduction process (**Figure 5(a)**, **(b)**, **(d)**, and **(e)**). Therefore, mild reduction and aging processes are necessary to increase the six-membered sp^2 carbon states as described in **Figure 5(d)**.

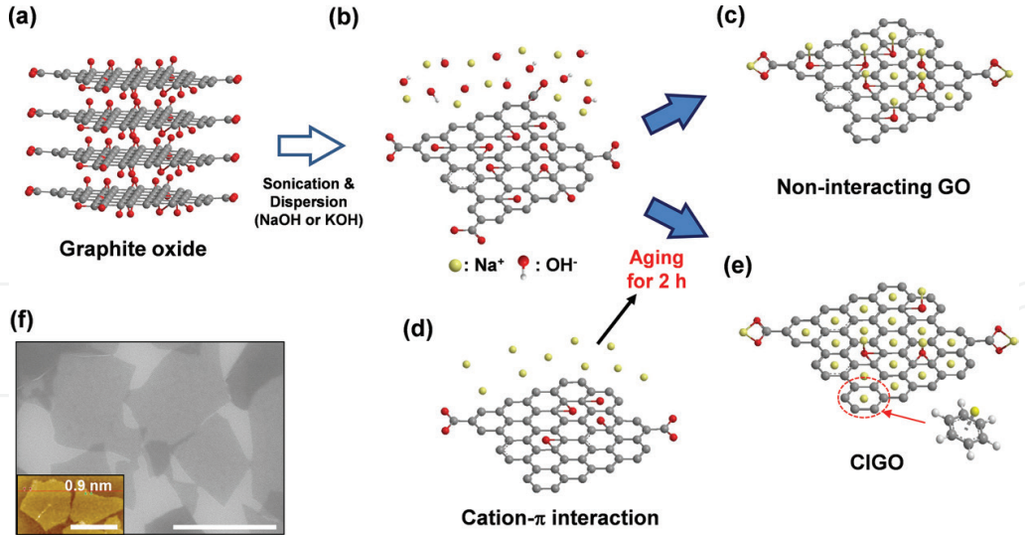

Figure 5. (a) Structure of graphite oxide, (b) as-exfoliated GO in NaOH solution, (c) highly interacting cations with oxygen functional groups. (a, b, d, e) procedure for obtaining the cation–π interacting GO. (d) Intermediate state of GO by mild deoxygenation aging in NaOH solution (e) decoration of cations on the partially reduced GO surface via a cation-π interaction. (f) FE-SEM image of CIGO on a silicon wafer (inset: AFM images of CIGO sheets). The scale bars in (f) and the inset are 2 μm [17].

Here, the electrostatic binding enthalpy of cations to a π system (−ΔH = 19.2 kcal/mol) was higher than that that of water (−ΔH = 17.9 kcal/mol). As the aging time is optimized, GO can be formed due to the cation interacting GO (CIGO) as shown in **Figure 5(e)**. Interestingly, the dispersion stability of noninteracting GO and CIGO were similar in aqueous solutions because of the presence of oxygen functional groups. However, the significant differences occurred after chemical reduction, which is described in **Figure 5(c)** and **(e)**. These results show that the cations with interacting sp^2 carbon did not desorb from the CIGO after the reduction process. Following the hydrazine reduction, the CIGO formed a dispersion of cation–π interacting RGO (CIRGO), whereas, the noninteracting GO aggregated in aqueous solution, as shown in **Figure 5(c)**. Moreover, the atomic force microscopy (AFM) image of the single-layered CIGO in **Figure 5(f)** confirmed its 2 μm size and 0.9 nm thickness.

3.3. Spontaneous reduction and dispersion of graphene oxide nanosheets with *in-situ* synthesized hydrazine assisted by hexamethyldisilazane

For real-life applications of RGO nanosheets, alcohol-based formulations of graphene are sometimes needed for graphene processing if the use of harsh organic solvents is not possible. Alcoholic solvents are not good for the dispersion of RGO in solutions due to their solubility parameters. Therefore, for the stable dispersion of RGO in alcoholic solvents, dispersant molecules should be added before the chemical reduction of GO in solutions. Recently, it has been reported that hexamethyldisilazane (HMDS) is a good candidate for the dispersion of RGO in alcohol because HMDS can be easily hydrolyzed into trimethylsilanol and ammonia in the presence of water. Furthermore, for the reduction of GO in solutions, hydrazine can be *in-situ* synthesized in a GO suspension by mimicking a typical reaction cycle involving GO (using alternative ketone molecules as catalysts) and ammonia and hydrogen peroxide as reagents.

Thus, HMDS can be used as a source of ammonia molecules for synthesizing hydrazine and dispersing RGO (**Figure 6**). The step-wise heating of the solution at 50 and 100°C is required to utilize keton groups in GO for in-situ synthesis of hydrazine molecules at high temperature for reduction of GO.

3.4. Dispersant-free dispersion of reduced graphene oxide by supramolecular chemistry

Highly concentrated colloidal suspensions of graphene nanosheets are of great interest for a variety of applications ranging from flexible electronics and conducting fibers to electrochemical electrodes for energy harvesting or storage devices. Unfortunately, many additives such as organic surfactants and polymeric dispersants should be added to prepare highly concentrated graphene pastes. These organic dispersant molecules can give detrimental effects on their electrical or thermal properties because graphene nanosheets can be separated by insulating organic materials if it is removed. Quadruple hydrogen bond (QHB) networks can overcome these issues for fabricating printable, spinnable, and chemically compatible conducting pastes containing high quality graphene nanosheets in organic solvents without the need for additional dispersion agents. Motivated by the self-assembly of donor-donor-acceptor-acceptor (DDAA) arrays of hydrogen bonding sites, GO nanosheets were functionalized

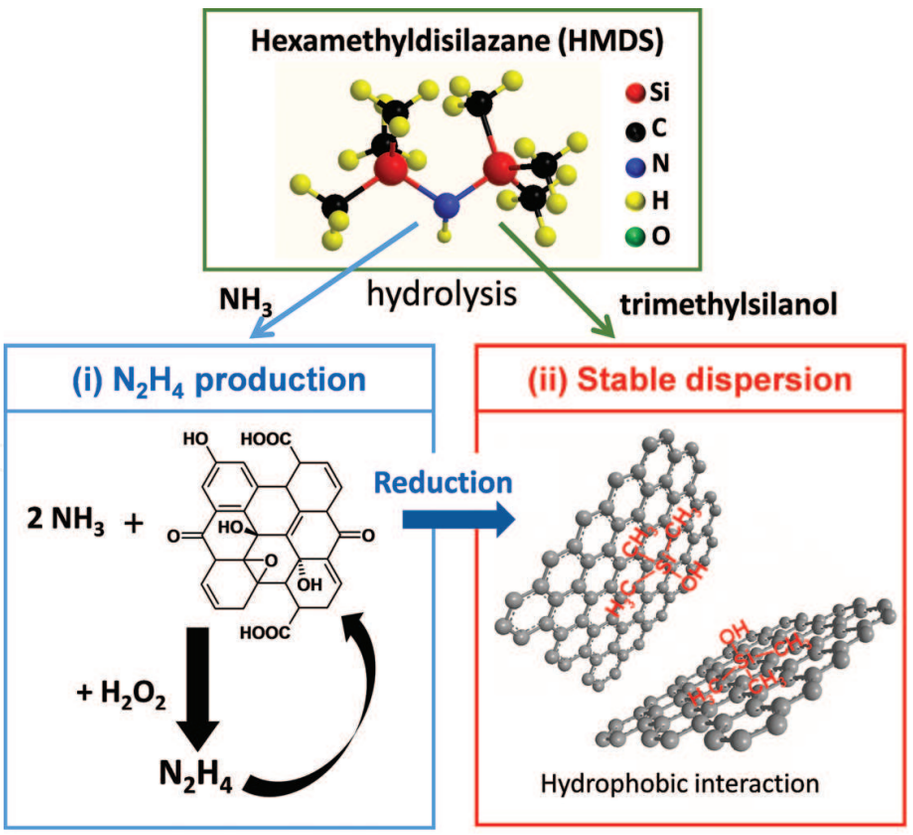

Figure 6. Roles of hexamethyldisilazane (HMDS): (i) ammonia source for the GO-assisted production of hydrazine upon the addition of hydrogen peroxide and (ii) RGO dispersion agent in ethanol, via hydrophobic interactions [18].

http://dx.doi.org/10.5772/intechopen.77284

using 2-ureido-4[1*H*]pyrimidinone (UHP) moieties to provide QHB motifs (**Figure 7(a)**). QHB arrays are much stronger than triple hydrogen bond arrays and are easily accessible synthetically. **Figure 7(b)** shows the well-dispersed RGO paste in DMF illustrating the striking synergy effect of QHB moieties into graphene nanosheets on the fabrication of dispersant-free RGO pastes. This unique paste can be used in electrochemical and printed electrodes and could be formed into flexible buckypaper.

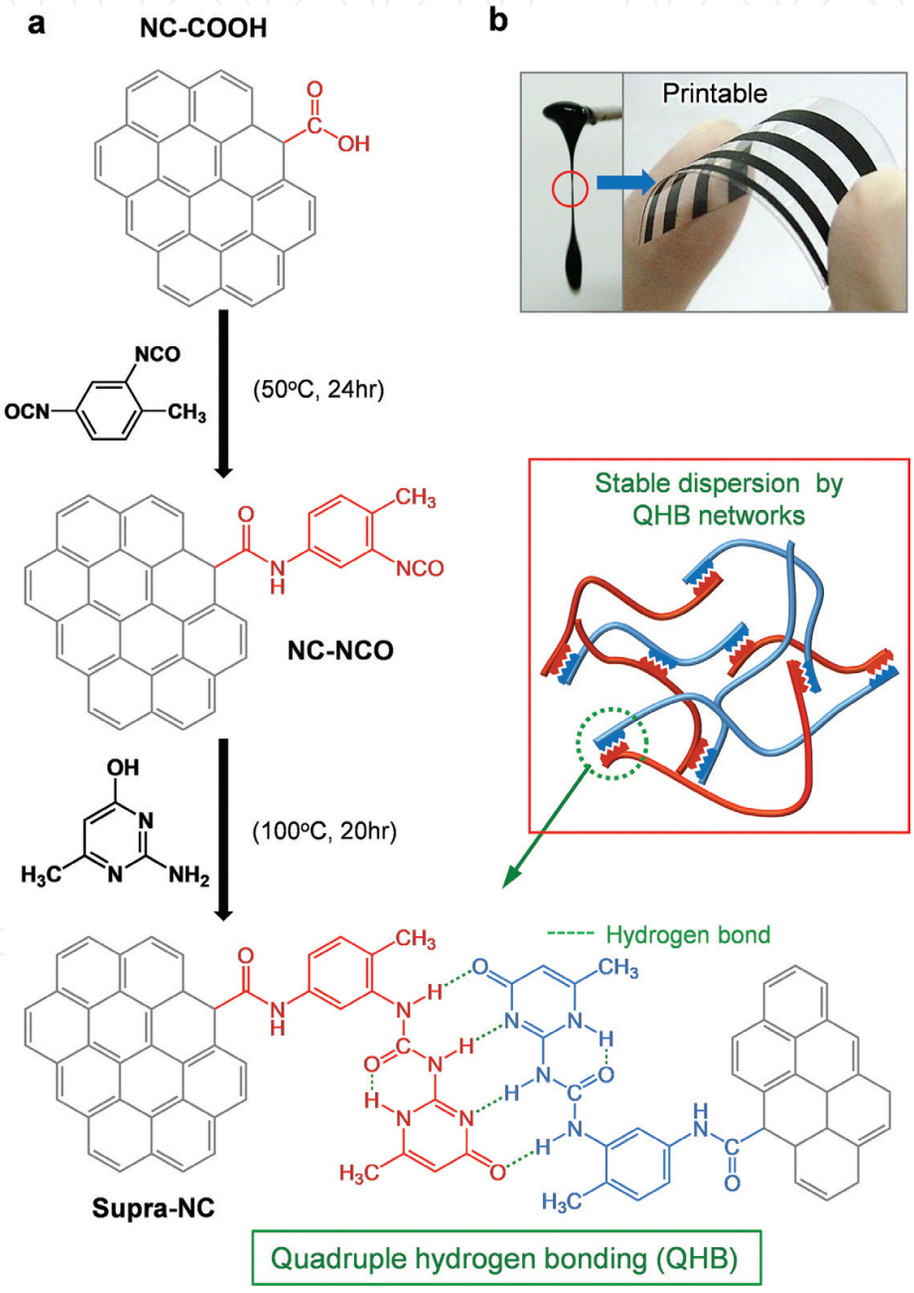

Figure 7. (a) Synthetic scheme for fabrication of graphene nanosheets functionalized with 2-ureido-4[*1H*]pyrimidinone moieties via a sequential reaction with toluene diisocyanate (TDI) and 2-amino-4-hydroxy-6-methyl-pyrimidine (AHMP) to form. (b) Photographs of well-dispersed RGO paste and printed electrode on the plastic substrate [19].

4. Graphene oxide nanosheets for surface and interfacial engineering

4.1. Atomically thin graphene oxide as a multifunctional dopant

Highly oxidized GO with electron-withdrawing groups can be utilized as a strong p-type dopant of nanocarbon materials such as carbon nanotubes (CNTs) and graphene because of the charge transfer interactions between sp^2 carbon and the oxidative functional groups in GO [20, 21]. Doping nanocarbon materials with GO nanosheets have advantages: stable and strong p-doping that maintains the intrinsic properties of pristine CNT films and chemical vapor deposition (CVD)-graphene. Controlling the surface wetting properties of nanocarbon films is very important for their use in optoelectronic devices, which are fabricated by layering a hydrophilic material on top of hydrophobic carbon electrodes. Moreover, deposited GO nanosheets on porous CNT networks can reduce the surface roughness of the film. Further, it is worth noting that the doping state assisted by GO nanosheets is stable for more than 40 days at room temperature and atmospheric pressure compared to that doped with nitric acid. **Figure 8** illustrates the advantage of GO nanosheets as p-type dopants for CVD-graphene. Graphene oxide doping decreased the sheet resistance of CVD-graphene from 600 to 292 Ω/sq. The doping effect of GO nanosheets on the CVD-graphene was demonstrated using Kelvin probe force microscopy (KPFM) and Raman spectroscopy results. The KPFM images associated with AFM images show that the surface potential of the graphene/single GO sheet is negatively shifted by 120 mV. The bright region in the Raman map of the 2D peak shows a p-doped area in a single GO nanosheet. The gate-dependent I-V characteristics of CVD-graphene and GO-doped CVD-graphene show that the hole mobility of CVD-graphene is almost unaffected by doping. The hole mobility of GO-coated graphene was found to be 3330 cm^2/Vs, which is only slightly lower than that of pristine graphene (under equivalent device positions before GO coating), 3500 cm^2/Vs. Graphene oxide nanosheets can be also used to modify the properties of single-walled carbon nanotube networks by p-doping, flattening the network surface, and making it hydrophilic. This is useful for fabricating optoelectronic devices onto GO modified graphene or single-walled carbon nanotube (SWCNT) films.

4.2. Graphene oxide as an interfacial modifier

For the fabrication of SWCNT patterns on hydrophilic substrates, partially reduced GO nanosheets are used as interfacial adhesive layers on hydrophilic SiO_2 surfaces. Hydrophobic materials can be easily detached from hydrophilic substrates. Thus, to obtain stable interfacial structure, hydrophilic substrates are usually treated with surface modifiers such as silane coupling agents. In this context, the deposition of GO onto substrates and its partial reduction has several advantages. The partially reduced GO having hydroxyl and carboxyl groups can play as a role of the interfacial adhesive between the substrate and the deposited materials. Moreover, this process is scalable and straightforward because uniform SWCNT networks can be formed even by spraying on plastic substrates. In terms of optoelectronic device application, partially reduced GO can be used for the work function engineering with the conducting and semiconducting materials. Uniform GO films and patterns can be fabricated by blow-assisted

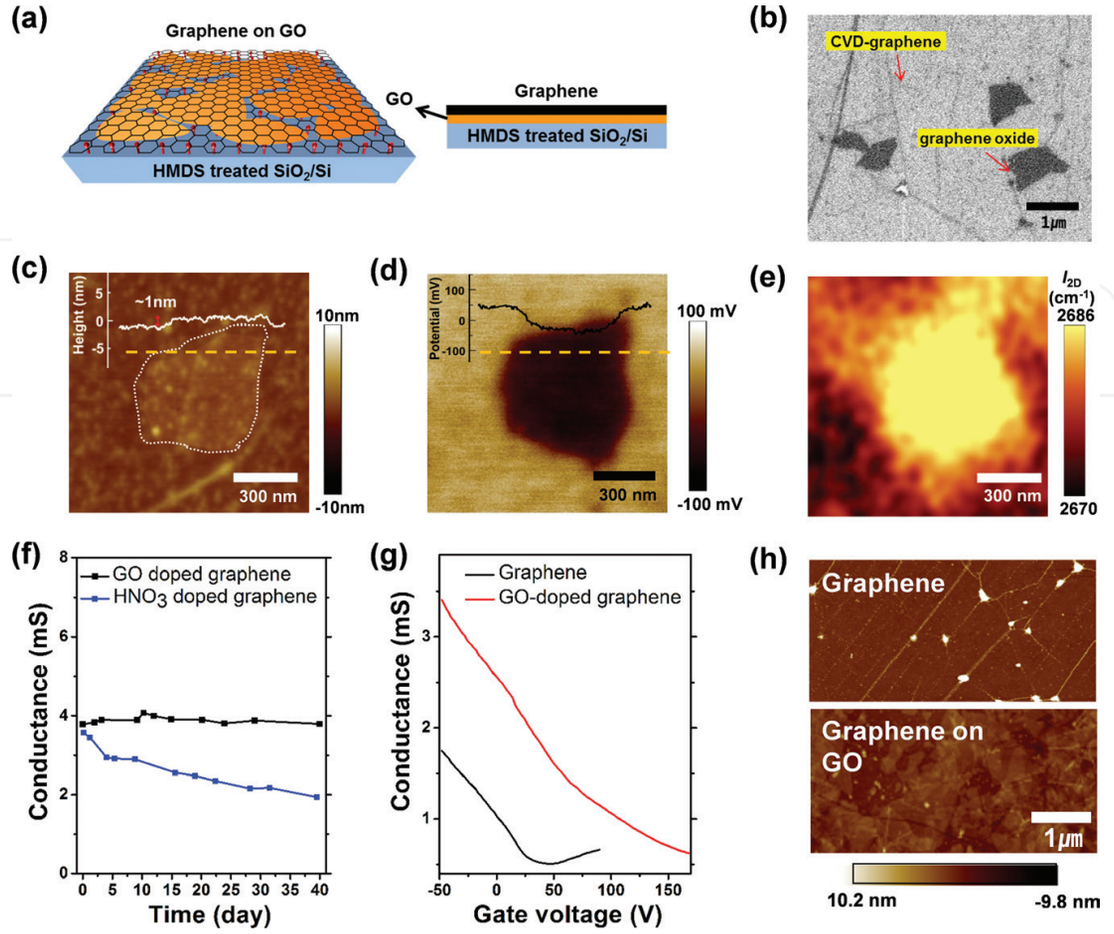

Figure 8. (a) Schematic diagram of graphene/GO film fabricated on an HMDS-treated SiO_2/Si substrate. (b) SEM image of CVD-grown graphene transferred on a GO sheet. (c) Atomic force microscope image and height profile showing the thickness of GO nanosheet, (d) kelvin probe force microscopy, and (e) Raman map of the 2D-band shift of CVD-grown graphene on a GO single sheet. (f) Electrical conductance variation of GO- and HNO_3-doped graphene with time at atmospheric pressure and room temperature. (g) Gate-dependent I-V characteristics of CVD-grown graphene and GO-doped graphene. (h) AFM images of CVD-grown graphene with and without GO [21].

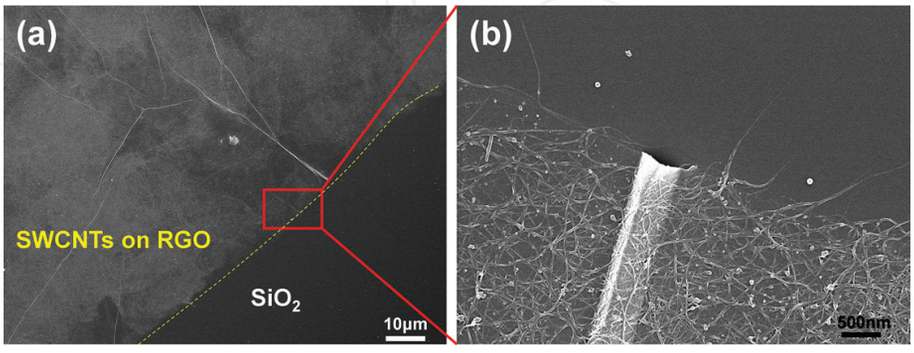

Figure 9. FESEM images of selectively deposited single-walled CNT films on partially reduced GO surfaces [22].

spin coating and inkjet printing, respectively, and the surface energy of the GO surface can be modulated by thermal treatment in vacuum. The SWCNTs were selectively deposited onto partially reduced GO films with moderately hydrophobic properties as shown in **Figure 9**.

5. Applications of graphene nanosheets in devices

5.1. Hierarchical graphene structure for lithium ion batteries

The hierarchical three-dimensional (3-D) structure for lithium ion battery (LIB) anodes has great potential for high electrochemical performances such as high-power densities and enhanced Coulomb's rates (C-rates). The efficient monolithic structure has a large specific surface area with numerous active sites, stable multistacking with short diffusion length, and high percolation threshold with high electrical conductivity as shown in **Figure 10(a)**. Unlike the porous-like graphene structuring on anode described in previous studies, monolithic graphene is similar to densely branched pine trees as shown in **Figure 10(b)**. The structure has high mechanical strength and flexibility, as well as high adhesion stability on the current collector. **Figure 10(c)** shows the growth mechanism for the structure by freeze-drying with water-soluble polymer [23]. The monolithic graphene anodes induced ultrafast charge/discharge rates with outstanding cycling stability with high capacitance as seen in **Figure 10(d)** and **(e)**. The fabrication method is simple and straightforward and suitable for high performance LIB anodes.

5.2. Fabrication of graphene oxide-based mid-IR detectors

Graphene oxide can be defined as chemically functionalized graphene containing oxygen. Moreover, GO has a large bandgap, which implies an insulating behavior. The bandgap can be decreased with decreasing the oxidation level of GO. Thus, this is a promising method for bandgap tuning that can be applicable to various optical and electronic devices. The spectrum ranges of GO-based photodetectors are limited within the visible and near-infrared (IR) wavelengths because they are based on the photovoltaic effect. Therefore, a new mechanism for mid-IR detection using GO sensors is required. Significantly, the control of oxygen functional

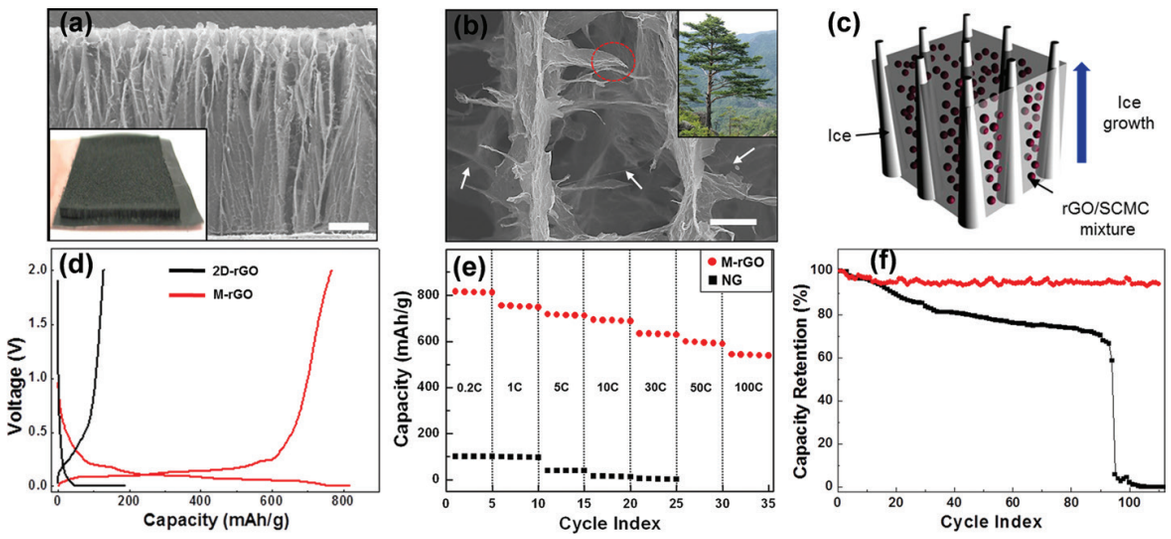

Figure 10. (a) FE-SEM image for monolithic RGO structure (inset: Vertically aligned RGO structure on current collector), (b) high magnification view of monolithic RGO, (c) growth mechanism for the monolithic structure during the freeze-drying process, (d) voltage profiles for monolithic-MGO (M-MGO) and 2-D RGO, (e) charge/discharge capacities for five cycles as the capacity rates increase from 0.2 to 100 C with respect to natural graphite and M-RGO, and (f) capacity retention for M-RGO (red line) and natural graphite (black line) [24].

groups in GO is possible for the application of IR detectors. (Bae et al. [25]) Here, GO is synthesized using thermal chemical vapor deposition (TCVD) and its electrical and optical properties are characterized using low-temperature measurements and Raman spectroscopy. The electrical conductivity of GO-based devices under IR irradiation was subsequently measured. The electrical characterization process can be described as follows. Single layered graphene (SLG) is synthesized on a copper substrate using the CVD method. Following its synthesis, the graphene is transferred onto SiO_2 substrate as shown in **Figure 11(a)**. Subsequently, SLG is deposited on a silicon substrate patterned using oxygen plasma etching. Furthermore, the metal electrode is deposited on the patterned substrate using Au as shown in **Figure 11(b)**. To produce GO, we performed chemical treatments using immersion in an aqueous acid solution as shown in **Figure 11(c)**. Subsequently, GO is cleaned with water to remove the residual acid and dried in vacuum as shown in **Figure 11(d)**. It should be noted that, in order to control the oxygen functional groups with certain resistance, it is reduced by annealing at optimum temperature as shown in **Figure 11(e)**. The optical microscopy image of the GO device is shown in **Figure 11(f)**. The dotted area indicates the fabricated GO channel between the metal electrodes.

Raman spectra illustrate the chemical doping effect by charge transfer between graphene and oxygen molecules. The spectra revealed significant changes in intensity ratio that can be described by the I(D)/I(G) and I(2D)/I(G) ratios. Moreover, the G band at 1590 cm^{-1} can be shifted due to the oxidation treatment. Four different samples: pristine CVD graphene, acid treated graphene, and annealed graphene after acid treatment are shown in **Figure 12(a)**. Initially, the I(D)/I(G) ratio increased after acid treatment compared to that of pristine graphene. This is caused by oxygen moieties generating intervalley scattering. After mild reduction by thermal treatment, the ratio decreases due to the partial elimination of oxygen functional groups. Thus, Raman spectra illustrate the doping effect of the oxygen functional groups. Moreover, charge transfer behavior presents as a p-type characteristic. The I(2D)/I(G) ratio is significantly decreased and the G band shows a red shift. Unlike graphene, GO has characteristic IR absorption peaks at

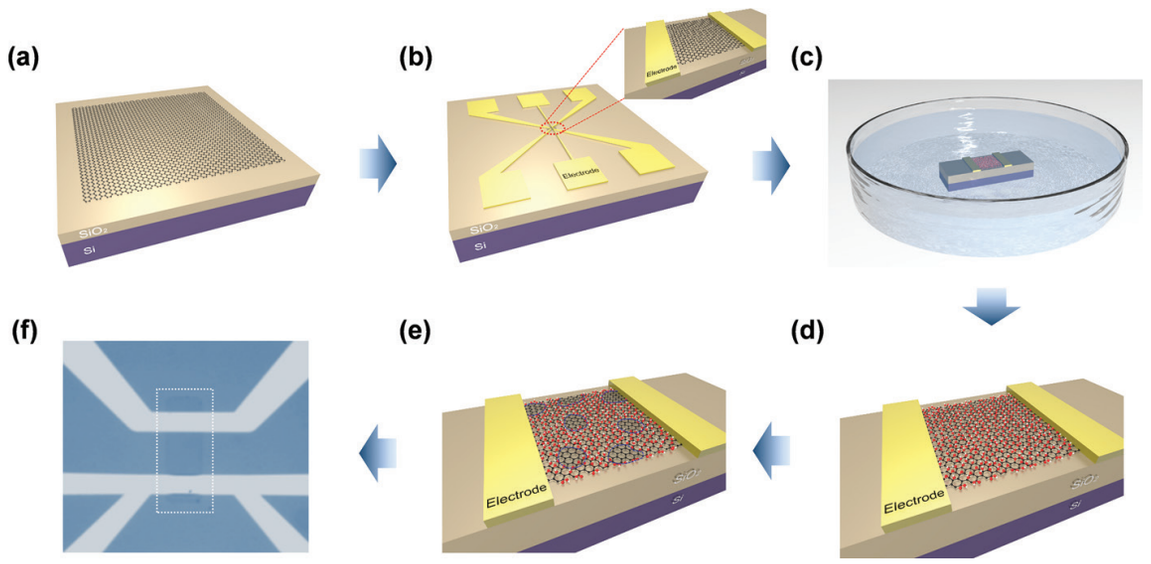

Figure 11. Fabrication schematics of the GO device: (a) transfer of CVD-grown graphene onto the Si/SiO_2 substrate, (b) patterning of graphene and deposition of electrodes, (c) acid treatment, (d) rinsing and drying, (e) reduction of GO, and (f) optical image of GO device [25].

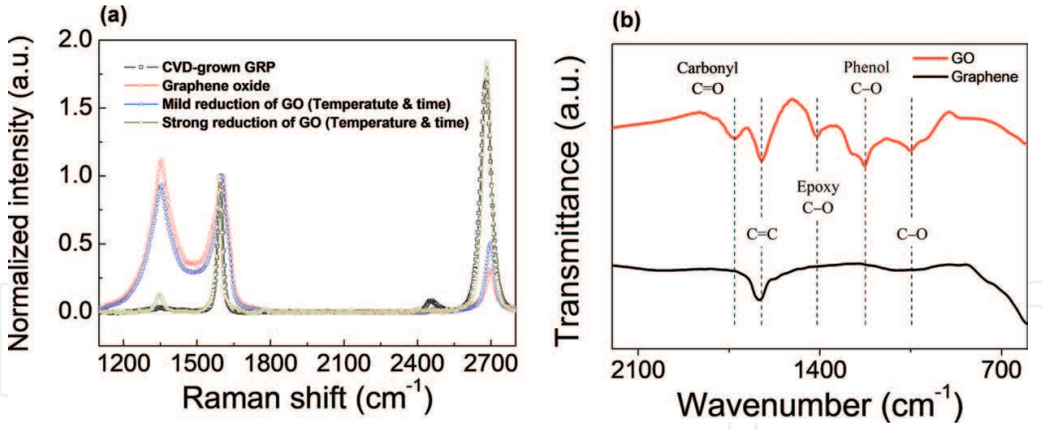

Figure 12. (a) Raman spectra of graphene, GO, and RGO and (b) IR absorption spectra of graphene and GO [25].

750–2250 cm^{-1}, as shown in **Figure 12(b)**. The Fourier transform infrared (FTIR) spectra of GO reveal oxygen functional groups from 960 to 1860 cm^{-1}, without graphene [26].

The optical properties of GO show in the mid-IR range at 7–14 μm. Depending on the functionality of GO by control of mild reduction, it reveals larger resistance changes as temperature. When the IR source is turned on, the resistance of the GO immediately drops from 31 to 7.4 MΩ, as shown in **Figure 13(a)**. This is a promising approach for obtaining sensitive mid-IR sensors by controlling GO functionalities. To describe the response of GO as a function of IR irradiation, the curve is fitted using nearest neighbor hopping (NNH) model as shown in **Figure 13(b)** and **(c)**. **Figure 13(c)** reveals a linear fit of ln(*G*)-T^{-1} in the 200–350 K temperature range, where G

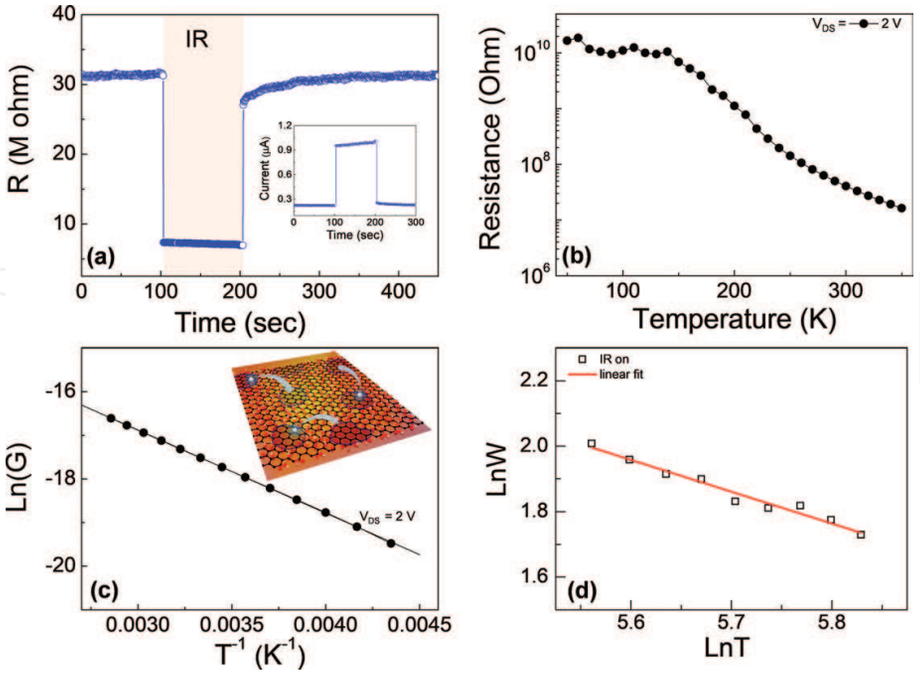

Figure 13. Electrical transport properties of GO under IR irradiation: (a) change in GO resistance, (b) GO resistance-temperature plot between 50 and 350 K, (c) temperature dependence of GO electrical conductance plotted for the NNH mechanism between 260 and 350 K, (d) ln(*W*) vs. ln(*T*) plot for GO [25].

is the conductance and T is the temperature. Consequently, under IR irradiation, NNH is more dominant than variable range hoping (VRH) in the electron transport of GO, which is usually observed at a higher temperature range in a disordered system, jumping electrons to other defect sites due to thermal activation. Therefore, the different nature of the electron transport induced by IR irradiation contributes to the different temperature dependence exhibited by *G*. The activation energy *W*, extracted from the slope of the plot in **Figure 13(c)** is approximately 164 meV. The energy is easily obtained by the incident IR. The specific NNH transport phenomena is confirmed by plotting ln(*W*) as a function of ln(*T*) as shown in **Figure 13(d)**. The temperature exponent is −0.97, indicating thermal transport in GO under IR irradiation. The plot exhibits a negative slope between 250 and 350 K. These results demonstrate that the conducting mechanism can be attributed to VRH. The shift from VRH to NNH transport occurs due to the increase in the temperature of GO due to the incident IR irradiation.

5.3. Graphene emitters

Controlling the structure of graphene emitters such as the aspect ratio, density, and alignment, which are of practical importance for applications in field emission devices, is not readily achievable. Jeong et al. introduced a simple method for fabricating tubular structured graphene arrays with controlled tube lengths and alignment as shown in **Figure 14**. They used the filtration of RGO suspensions with a polycarbonate membrane. The interactions between hydrophobic graphene and the pore walls, but not the top surfaces, of a polycarbonate membrane were tuned, and the filtration rate was varied to control the length and alignment of the graphene arrays. They observed that the lengths of the graphene arrays increased with increasing filtration rate, but a maximum field emission efficiency was reached for intermediate filtration rates due to field screening for array lengths longer than an optimum value. The turn-on field and field enhancement factor for an optimum length of graphene arrays were 1.89 V/μm and 4624, respectively.

Another useful approach for fabricating graphene field emitters is a thermal welding-peeling method as shown in **Figure 15**. The graphene film was formed on a polytetrafluoroethylene membrane by filtering the dispersed RGO solutions. The CNT/polyethersulfone (PES)

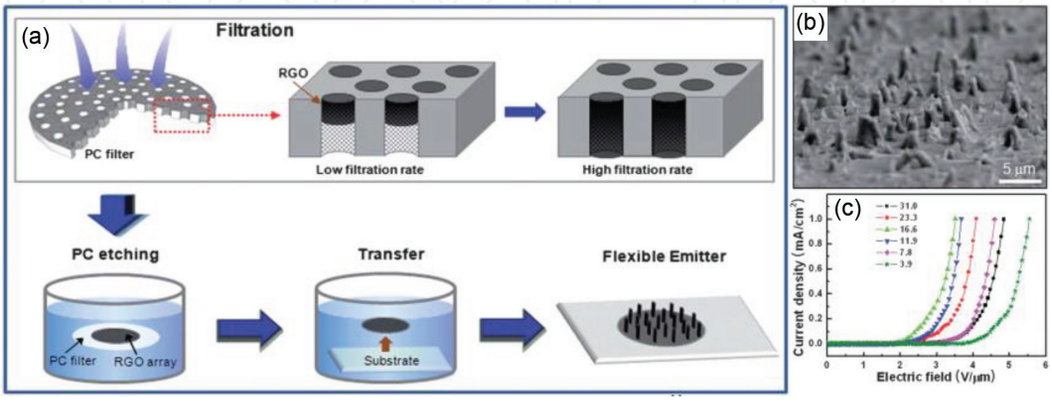

Figure 14. (a) Schematic and (b) SEM image of RGO emitters fabricated by filtration-transfer method. (c) J-E curves of RGO emitters as a function of filtration rate [27].

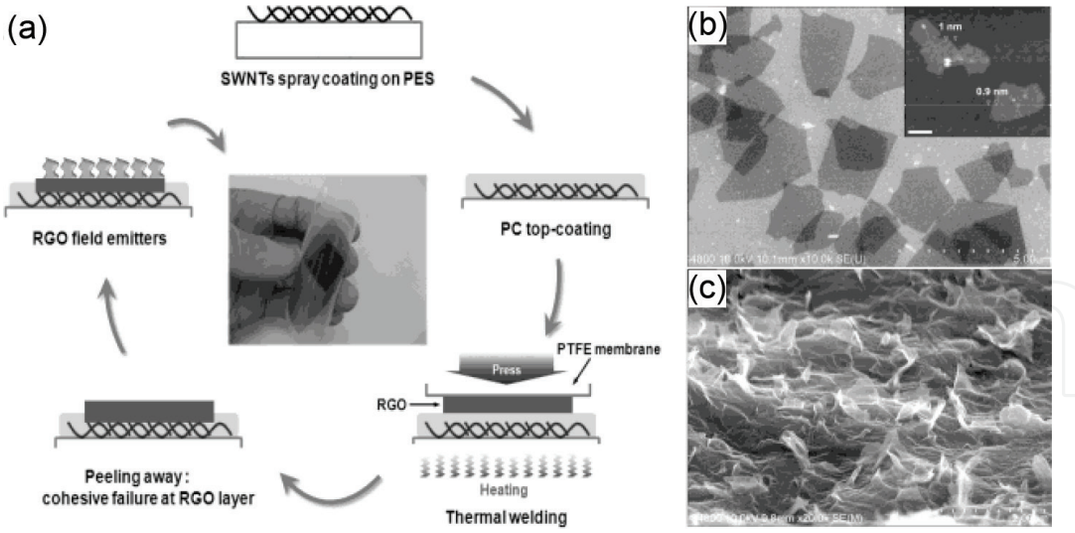

Figure 15. (a) Schematic diagram of RGO emitters fabricated using a thermal welding-peeling technique. SEM image of (b) RGO sheets and (c) fabricated RGO emitters [28].

substrate used as cathode was then coated with an adhesive polycarbonate layer to prepare an upper graphene thin film under pressed thermal treatment of the sample. Vertically aligned graphene emitters were finally constructed by peeling off the polytetrafluoroethylene membrane from the welded sample. The average height and interspace of graphene emitters were 1.2 and 0.8 μm, respectively, which could be controlled by experimental conditions such as the size of the GO sheets and peeling force of the membrane. A large field enhancement factor for the RGO emitters was achieved by optimum vertical alignment of GO nanosheets, resulting in a high emission current density and a low turn-on field.

The "breath figure" technique is a simple and versatile self-assembly method for fabricating porous nanomaterial patterns with high regularity. Although highly ordered 3-D graphene assemblies with high porosity have been fabricated, their use for field emitters was not readily achieved because the flat or smooth surface structures of the graphene assemblies did not emit electrons. Vertically aligned graphene ordered structures for an efficient field emitter was first fabricated using the "breath figure" method as shown in **Figure 16**. Octadecylamine (ODA)-functionalized GO solution dispersed in toluene was uniformly coated onto a substrate by spin coating. The ODA-functionalized GO was self-assembled under high humidity conditions and presented high periodicity due to the surface energy difference between the water droplet and toluene. Moreover, the ODA-functionalized GO nanosheets tended to encapsulate water droplets and precipitate at the water–solution interface, thereby preventing coalescence of the water droplets. The patterned ODA-functionalized GO array structure was obtained after the complete evaporation of the toluene and water droplets. The structure of GO array, the size, shape, and homogeneity, was dependent on the viscosity of the ODA-functionalized GO solution, large hexagonally structured GO patterns were fabricated with solutions having a low viscosity. The vertically aligned tip structures were formed at the interfaces between pores. However, with highly viscous solutions, small spherical patterns generated without tip formation. The graphene array prepared using a 2.0 g/L GO solution displayed the lowest turn-on field of 2.04 V/μm of all the arrays prepared using various GO concentrations.

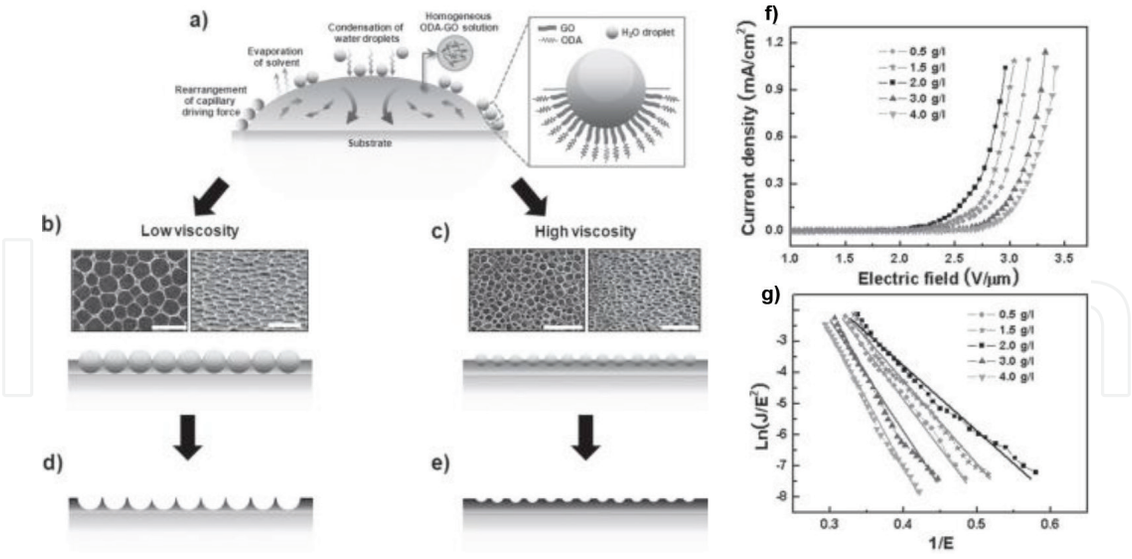

Figure 16. (a) Schematic diagram of the graphene arrays obtained using the 'breath figure" method, and pattern structures obtained at (b) and (d) low and (c) and (e) high solution viscosities, respectively. (f) J-E and (g) F-N plots of graphene arrays fabricated using various GO concentrations [29].

Freeze-drying of highly concentrated water-based RGO/polymer paste is one of the fabricating methods for 3-D graphene emitters with random micropores. Kim et al. first reported 3-D monolithic graphene structures as shown in **Figure 17**. They used highly concentrated water-based RGO paste prepared using monovalent cation-π interactions. After bar coating the paste on substrate, freezing was performed by immersing the sample in a liquid nitrogen bath. Low temperature freezing using liquid nitrogen resulted in the rapid formation of ice nuclei, hence the growth of relatively small ice crystals. After the sublimation of the ice crystals by vacuum drying, monolithic 3-D graphene structures with cylindrical pores could be obtained. Although the randomly distributed pores of the 3-D graphene structure were

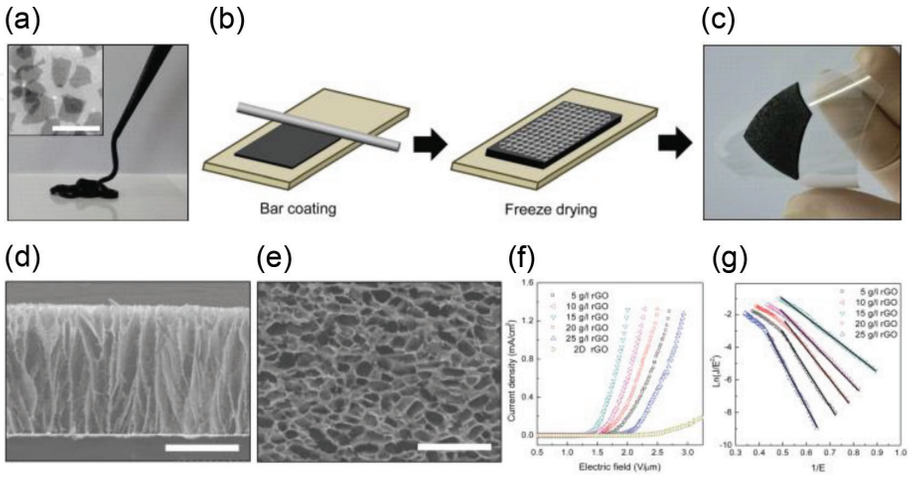

Figure 17. (a) Photo image of a water-based RGO paste. Inset shows the SEM image of the RGO sheets. The scale bar is 5 μm. (b) Fabrication method of the monolithic 3-D graphene structure using bar coating of the RGO paste, followed by subsequent freeze-drying. (c) a 3-D structured graphene fabricated on a plastic substrate. (d) Cross-sectional and (e) top view SEM images of a 3-D graphene structure. The scale bars are 300 μm. (f) J–E and (g) F-N plots of the 3-D graphene emitters as a function of graphene concentrations [30].

several tens of micrometers in size, the pore walls had numerous sharp edges. The size, shape, and homogeneity of these pores could be adjusted by choosing different freezing temperatures, solution concentrations, and solvents.

The tunneling barrier at the interface between a material surface and vacuum can be modulated by varying the physical properties of an emitter material. In this context, the field-emission characteristics are critically dependent on the work function of an emitter material. Low work functions decrease the barrier height causing the enhancement of electron tunneling for a given applied electric field, which results in high field-emission characteristics. Chemical doping can be a useful approach for modulating the work function of graphene because the intrinsic Fermi level of graphene can be readily shifted, due to charge transfer between the dopant and graphene. Jeong et al. reported the work-function engineering of graphene field emitters using chemical doping. Gold chloride as a p-type dopant and aluminum chloride powder as an n-type dopant were dissolved in distilled water and mixed with a GO solution. After centrifugation, the solution was filtered and the doped graphene films were dried. The schematic diagram in **Figure 18** shows the charge transfer from graphene to the gold and aluminum ions and the corresponding band diagrams. The charge transfer upon chemical doping was confirmed using various techniques such as Raman, X-ray photoelectron spectroscopy (XPS), and ultraviolet photoelectron spectroscopy (UPS). Due to decreasing the work-function of graphene, the Al-doped graphene emitters showed lower turn-on field than those of undoped and Au-doped graphene emitters. A similar study was conducted by mixing dopant solution with graphene paste.

Long-term emission stability of electron emitters is needed for thigh quality field emission devices. The ion bombardment of residual gas species which are degassed from cathodes,

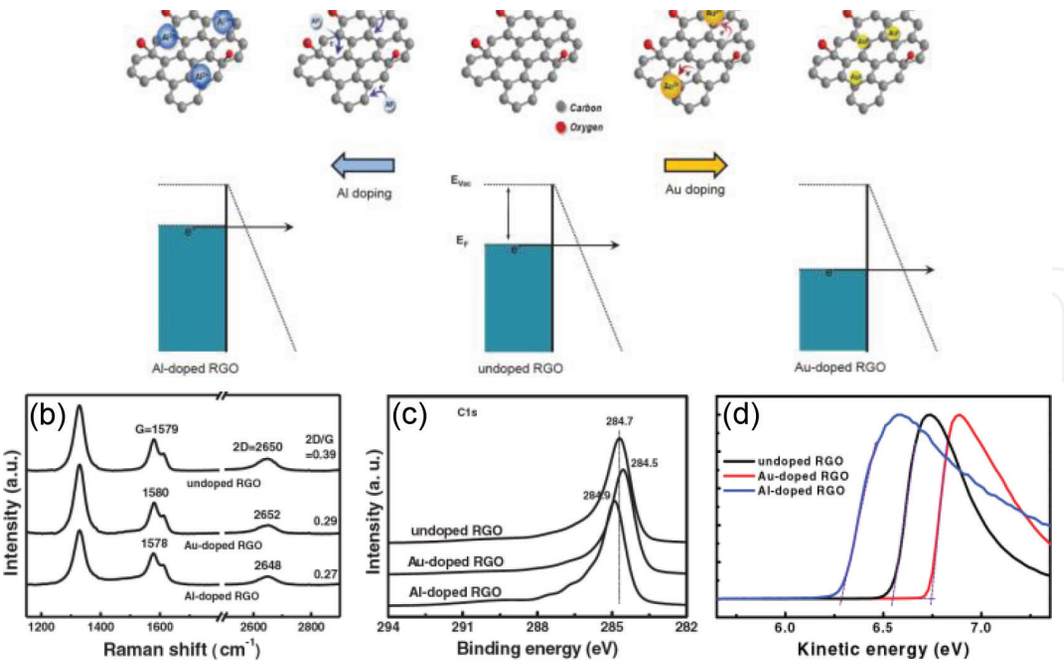

Figure 18. (a) Schematic diagram showing the electron transfer from graphene to the Au ion and from Al to graphene and corresponding band diagrams under application of a certain external voltage. (b) Raman, (c) XPS, and (d) UPS spectra for the undoped, Au-doped, and Al-doped graphene emitters [28].

getters, inner walls, and phosphors can destruct electron emitters, resulting in a critical reduction of the emitter characteristics. To enhance the current stability, Jeong et al. introduced the ZnO sol coating as a protective layer for the RGO emitters as shown in **Figure 19** [27]. Zinc oxide is an n-type semiconductor with a wide band gap and a low resistivity in the order of 10^{-2} to 10^{-3} Ω cm. The ZnO layer on the graphene surface was realized by hydrogen bonding between the amine groups of the ZnO sol and carboxyl groups of RGO and subsequent thermal treatment. A life time test showed stable emission for the ZnO-coated graphene emitters, which might be due to the ZnO protection of the emission site from reactive ion bombardment.

Since the development of graphene-based thin film fabrication techniques on polymeric substrates, research into graphene-based flexible electrodes for display application has advanced. In addition to the high electrical and mechanical flexibility of graphene-based thin films, the interface between an electrode and an emitter material should be strong and provide ohmic contact to achieve highly flexible field emitters. Thus, SWNT-coated polymer substrates have been used as electrodes [31]. Moreover, RGO emitters were fabricated on SWNT-coated PET substrates. A

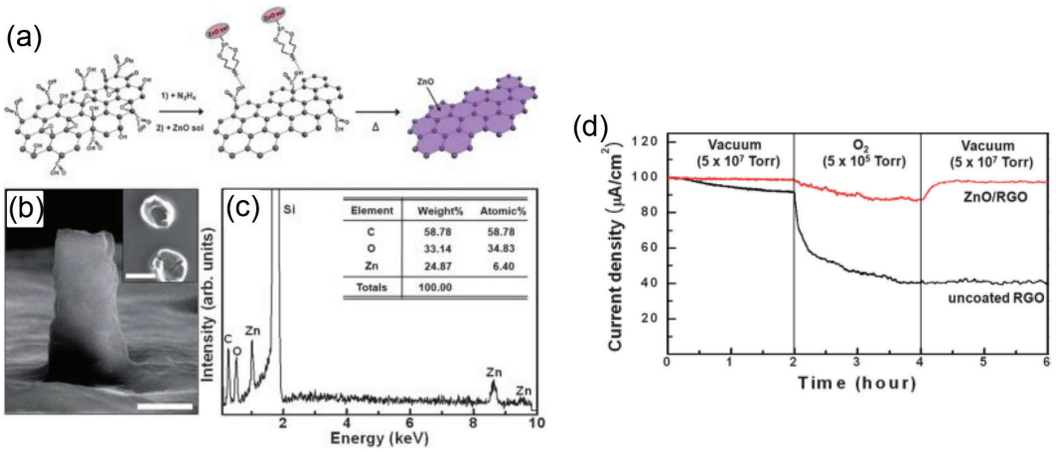

Figure 19. (a) Illustration of formation of a ZnO protective layer on the RGO surface. (b) SEM images and (c) EDAXS plot of the RGO emitters modified with a ZnO layer. Scale bars in (b) are 5 μm. (d) Current stability of the RGO array emitters wit and without a ZnO layer in vacuum and after exposure to O_2 [27].

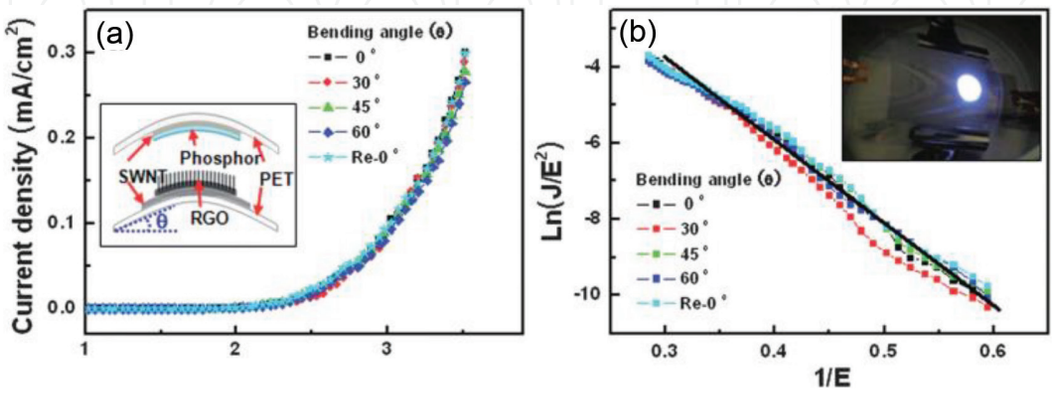

Figure 20. (a) J–E and (b) F–N plots of the RGO emitters as a function of the bending angle. The insets show schematic diagrams of the flexible field emission setup and an emission pattern at a 30° bending angle, respectively [26].

PET film was used as the spacer and a white phosphor-coated SWNT layer on a PET substrate was used as the anode as shown in **Figure 20**. Strong π-π carbon bonds allowed the RGO arrays to form strong mechanical contact with the SWNT network. The emission current density of the RGO emitters did not decrease much with increasing the bending angle. This stable emission is likely due to the strong adhesion of the 3-D RGO emitters to the SWNT-coated PET substrate.

6. Summary

We have briefly reviewed the recent research progress on chemically exfoliated graphene nanosheets via graphite oxide exfoliation and chemical reduction. Efficient graphite oxide exfoliation methods were developed by using homogenizers for shearing in solution and unusual horn sonication for stable acoustic cavitation. These methods show promise for fabricate improved GO nanosheets for high performance RGO nanosheets for conductor or electrochemical electrode applications. Highly oxidized GO nanosheets were utilized for p-type doping of CNTs and graphene films as well as for surface energy modifications. The modulation of the surface energy of GO can also allow us to deposit hydrophobic materials on hydrophilic surfaces. Strategies for the stable dispersion of RGO nanosheets in solution included sol–gel chemistry, cation-π interaction, supramolecular chemistry, and so on. Both GO and RGO nanosheets can be used as mid-IR detector, field emitters, 0r as electrodes in energy storage devices. Although some fascinating results have been achieved in previous publications, studying the fundamental and practical properties of GO or RGO should continue because their properties are critically dependent on the oxidation process of graphite, exfoliation method, reduction, and so on. Future applications of chemically exfoliated graphene in soft electronics, nanostructure control and hybridization with other materials are yet a challenge for high performance in real-life applications.

Acknowledgements

This work was supported by the Center for Advanced Soft-Electronics as Global Frontier Project (2014M3A6A5060953) and Nano-Material Technology Development Program (2016M3A7B4021151) funded by the Ministry of Science, ICT and Future Planning and by the Primary Research Program (18-12-N0101-16/18) of the Korea Electrotechnology Research Institute.

Author details

Joong Tark Han*, Seung Yol Jeong, Hee Jin Jeong and Geon-Woong Lee

*Address all correspondence to: jthan@keri.re.kr

Korea Electrotechnology Research Institute, Republic of Korea

References

[1] Eda G, Unalan HE, Rupesinghe N, Amaratunga GAJ, Chhowalla M. Field emission from graphene based composite thin films. Applied Physics Letters. 2008;**93**:233502. DOI: 10.1063/1.3028339

[2] Loh KP, Bao Q, Eda G, Chhowalla M. Graphene oxide as a chemically tunable platform for optical applications. Nature Chemistry. 2010;**2**:1015-1024. DOI: 10.1038/nchem.907

[3] El-Kady MF, Strong V, Dubin S, Kaner RB. Laser scribing of high-performance and flexible graphene-based electrochemical capacitors. Science. 2012;**16**:1326-1330. DOI: 10.1126/science.1216744

[4] Dreyer DR, Park S, Bielawski CW, Ruoff RS. The chemistry of graphene oxide. Chemical Society Reviews. 2010;**39**:228-240. DOI: 10.1039/B917103G

[5] Brodie BC. On the atomic weight of graphite. Philosophical Transactions of the Royal Society of London. 1859;**149**:249-259. DOI: 10.1098/rstl.1859.0013

[6] Staudenmaier L. Verfahren zur Darstellung der Graphitsaure. Berichte der Deutschen Chemischen Gesellschaft. 1898;**31**:1481-1499. DOI: 10.1002/cber.18980310237

[7] Hummers JWS, Offeman RE. Preparation of graphitic oxide. Journal of the American Chemical Society. 1958;**80**:1339. DOI: 10.1021/ja01539a017

[8] Park S, Ruoff RS. Chemical methods for the production of graphenes. Nature Nanotechnology. 2009;**4**:217-224. DOI: 10.1038/nnano.2010.69

[9] Jeong SY, Kim SH, Han JT, Jeong HJ, Yang S, Lee G-W. High performance transparent conductive films with rheologically-derived reduced graphene oxide. ACS Nano. 2011; **5**:870-878. DOI: 10.1021/nn102017f

[10] Li JL, Kudin KN, McAllister MJ, Prud'homme RK, Aksay IA, Car R. Oxygen-driven unzipping of graphitic materials. Physical Review Letters. 2006;**96**:176101. DOI: 10.1103/PhysRevLett.96.176101

[11] Ajayan PM, Yakobson BI. Materials science: Oxygen breaks into carbon world. Nature. 2006;**441**:818-819. DOI: 10.1038/441818a

[12] Xu H, Zeiger BW, Suslick KS. Sonochemical synthesis of nanomaterials. Chemical Society Reviews. 2013;**42**:2555-2567. DOI: 10.1039/C2CS35282F

[13] Han JT, Jeong JI, Kim HK, Hwang JY, Yoo HK, Woo JS, Choi S, Kim HY, Kim HJ, Jeong HJ, Jeong SY, Baeg K-J, Cho K, Lee G-W. Extremely efficient liquid exfoliation and dispersion of layered materials by unusual acoustic cavitation. Scientific Reports. 2014;**4**:5133. DOI: 10.1038/srep05133

[14] Manga KK, Wang S, Jaiswal M, Bao Q, Loh KP. High-gain graphene-titanium oxide photoconductor made from inkjet printable ionic solution. Advanced Materials. 2010; **22**:5265-5270. ISSN 0935-9648

[15] Han JT, Kim BG, Yang M, Kim JS, Jeong HJ, Jeong SY, Hong SH, Lee GW. Titania-assisted dispersion of carboxylated single-walled carbon nanotubes in a ZnO sol for transparent conducting hybrid films. ACS Applied Materials & Interfaces. 2011a;**3**:2671-2676 ISSN 1944-8244

[16] Han JT, Kim BJ, Kim BG, Kim JS, Jeong BH, Jeong SY, Jeong HJ, Cho JH, Lee G–W. Enhanced electrical properties of reduced graphene oxide multilayer films by in-situ insertion of a TiO_2 layer. ACS Nano. 2011;**5**:8884-8891. DOI: 10.1021/nn203054t

[17] Jeong SY, Kim SH, Han JT Jeong HJ, Jeong SY, Lee G-W. Highly concentrated and conductive reduced graphene oxide nanosheets by cation-π interaction: Toward printed electronics. Advanced Functional Materials. 2012;**22**:3307-3314. DOI: 10.1002/adfm.201200242

[18] Han JT, Jang JI, Jeong BH, Kim BJ, Jeong SY, Jeong HJ, Cho JH, Lee G–W. Spontaneous reduction and dispersion of graphene nano-platelets with in situ synthesized hydrazine assisted by hexamethyldisilazane. Journal of Materials Chemistry. 2012;**22**:20477-20481. DOI: 10.1039/C2JM34691E

[19] Han JT, Jeong BH, Seo SH, Roh KC, Kim S, Choi S, Woo JS, Kim HY, Jang JI, Shin D-C, Jeong S, Jeong HJ, Jeong SY, Lee G-W. Dispersant-free conducting pastes for flexible and printed nanocarbon electrodes. Nature Communications. 2013;**4**:2491. DOI: 10.1038/ncomms3491

[20] Han JT, Kim JS, Jo SB, Kim SH, Kim JS, Kang B, Jeong HJ, Jeong SY, Cho K, Lee G-W. Graphene oxide as a multi-functional p-dopant of transparent single-walled carbon nanotube films for optoelectronic devices. Nanoscale. 2012;**4**:7735-7742. DOI: 10.1039/C2NR31923C

[21] Kim H, Kim HH, Jang JI, Lee SK, Lee G–W, Han JT, Cho K. Doping graphene with an atomically thin two dimensional molecular layer. Advanced Materials. 2014;**26**:8141-8146. DOI: 10.1002/adma.201403196

[22] Han JT, Kim JS, Kwak D, Kim BG, Jeong BH, Jeong SY, Jeong HJ, Cho K, Lee G-W. Transparent carbon nanotube patterns templated by inkjet-printed graphene oxide nanosheets. RSC Advances. 2011;**1**:44-47. DOI: 10.1039/C1RA00213A

[23] Zhang H, Hussain I, Brust M, Butler M, Rannard SP, Cooper AI. Aligned two- and three-dimensional structures by directional freezing of polymers and nanoparticles. Nature Materials. 2005;**4**:787-793. DOI: 10.1038/nmat1487

[24] Jeong SY, Yang S, Jeong S, Kim IJ, Jeong HJ, Han JT, Baeg KJ, Lee GW. Monolithic graphene trees as anode material for Lithium ion batteries with high C-rates. Small. 2015;**11**:2774-2781. DOI: 10.1002/smll.201403085

[25] Bae JJ, Yoon JH, Jeong S, Boon BH, Han JT, Jeong HJ, Lee G-W, Hwang HR, Lee YH, Jeong SY, Lim SC. Sensitive photo-thermal response of graphene oxide for mid-infrared detection. Nanoscale. 2015;**7**:15695-15700. DOI: 10.1039/C5NR04039F

[26] Acik M, Lee G, Mattevi C, Chhowalla M, Cho K, Chabal YJ. Unusual infrared-absorption mechanism in thermally reduced graphene oxide. Nature Materials. 2010;**9**:840-845. DOI: 10.1038/nmat2858

[27] Jeong HJ, Jeong HD, Kim HY, Kim SH, Kim JS, Jeong SY, Han JT, Lee G-W. Flexible field emission from thermally welded chemically doped graphene thin films. Small. 2012;**8**:272-280. DOI: 10.1002/smll.201101696

[28] Jeong HJ, Kim HY, Jeong HD, Jeong SY, Han JT, Lee G-W. Arrays of vertically aligned tubular-structured graphene for flexible field emitters. Journal of Materials Chemistry. 2012;**22**:11277-11283. DOI: 10.1039/C2JM31263H

[29] Jeong HJ, Jeong HD, Kim HY, Jeong SY, Han JT, Lee G-W. Self-organized graphene nanosheets with corrugated, ordered tip structures for high-performance flexible field emission. Small. 2013;**9**:2182-2188. DOI: 10.1002/smll.201202143

[30] Kim HY, Jeong S, Jeong SY, Baeg K-J, Han JT, Jeong MS, Lee G-W, Jeong HJ. Chemically doped three-dimensional porous graphene monoliths for high-performance flexible field emitters. Nanoscale. 2015;**7**:5495-5502. DOI: 10.1039/C4NR07189A

[31] Jeong HJ, Jeong HD, Kim HY, Kim JS, Jeong SY, Han JT, Bang DS, Lee G-W. All-carbon nanotube-based flexible field-emission devices: From cathode to anode. Advanced Functional Materials. 2011;**21**:1526-1532. DOI: 10.1002/adfm.201001469

IntechOpen